Polymer 51 (2010) 3532–3539

Contents lists available at ScienceDirect

Polymer

journal homepage: www.elsevier.com/locate/polymer

Effects of sodium and zinc neutralization on large deformation hysteresis of an ethylene methacrylic acid butyl acrylate copolymer

B.P. Greviskes [a], K. Bertoldi [a,d], S. Deschanel [a], S.L. Samuels [c], D. Spahr [c], R.E. Cohen [b], M.C. Boyce [a,*]

[a] Department of Mechanical Engineering, Massachusetts Institute of Technology, 77 Massachusetts Avenue, Cambridge, MA 02139, USA
[b] Department of Chemical Engineering, Massachusetts Institute of Technology, USA
[c] E.I. du Pont de Nemours and Company, Inc., Wilmington, DE, USA
[d] School of Engineering and Applied Sciences, Harvard University, Cambridge, MA 02138, USA

ARTICLE INFO

Article history:
Received 19 November 2009
Accepted 29 April 2010
Available online 21 May 2010

Keywords:
Neutralization
Dissipation
Rate dependence
Ionomers

ABSTRACT

The mechanical hysteresis and recovery behaviors of an elastomeric ethylene methacrylic acid butyl acrylate (EMAABA) copolymer, its sodium-neutralized ($EMAABA_{Na}$) and zinc-neutralized ($EMAABA_{Zn}$) counterparts are evaluated and compared under large strain loading conditions. Experiments at different rates, under cyclic loading conditions and in relaxation indicate two major hysteresis mechanisms: a characteristic viscoelastic mechanism operative at all strains and a microstructural evolution/breakdown mechanism incurred during large strains. Loading-unloading cycles show large rate-dependent hysteresis loops with significant recovery of strain upon unloading, revealing a highly dissipative yet resilient behavior. The microstructure breakdown mechanism occurs during the initial strain excursion as revealed by subsequent loading cycles showing a significantly more compliant behavior and dramatically reduced hysteresis loops. The neutralized materials are found to be significantly stiffer, stronger and more dissipative compared to the neat material while still retaining the same level of recovery. Therefore the neutralization of this material provides an excellent means to tune stiffness and dissipation while retaining resilience, providing mechanical performance properties attractive for abrasion, impact and puncture resistant applications.

1. Introduction

Ionomers are polymers possessing ionic functional groups pendant to the polymer backbone [1]. Ethylene methacrylic acid (EMAA) and ethylene methacrylic acid butyl acrylate (EMAABA) copolymers neutralized with sodium, magnesium, or zinc cations form a class of ionomers with an outstanding combination of mechanical properties, including stiffness, strength, toughness, resilience (i.e., recovery of strain upon unloading), abrasion resistance and puncture resistance [2,3]. These properties can be tuned by varying the relative amounts of amorphous domains, crystalline domains and ionic aggregates, with the resulting range in mechanical properties being remarkably broad [4–6]. This range in properties can be further broadened by changing the type and concentration of ionic aggregates, and their distribution along the polymer chain backbone [1,7].

Previous mechanical studies have investigated the dynamic mechanical properties [8], the yielding [7,9], and the large deformation and rate-dependent behaviors [10] of EMAA [7–9] and EMAABA [10]. However, a detailed characterization of the dissipative nature of these materials at large strain has not been conducted. Due to the use of these materials as cut-resistant coatings, puncture-resistant packagings and impact absorbing materials, the dissipation and resilience upon large strain deformation are governing behaviors for application. Thus, it is important to understand how neutralization affects the dissipation and recovery. In this paper, we study an ethylene methacrylic acid butyl acrylate copolymer (EMAABA) both in its neat (non-neutralized) and neutralized forms – here the homopolymer is neutralized with Sodium ($EMAABA_{Na}$) and Zinc ($EMAABA_{Zn}$). These three copolymers are studied in their elastomeric regime of behavior (at 25 °C) in large deformation uniaxial compression over a wide range of strain rates (from $10^{-4}\,s^{-1}$ to $9000\,s^{-1}$); results from monotonic loading tests, cyclic tests and relaxation tests are presented, as well as results from small strain dynamic mechanical analysis. The results are used to characterize the effects of neutralization on the dissipative character of the homopolymer.

* Corresponding author.
E-mail address: mcboyce@mit.edu (M.C. Boyce).

0032-3861/$ – see front matter © 2010 Elsevier Ltd. All rights reserved.
doi:10.1016/j.polymer.2010.04.066

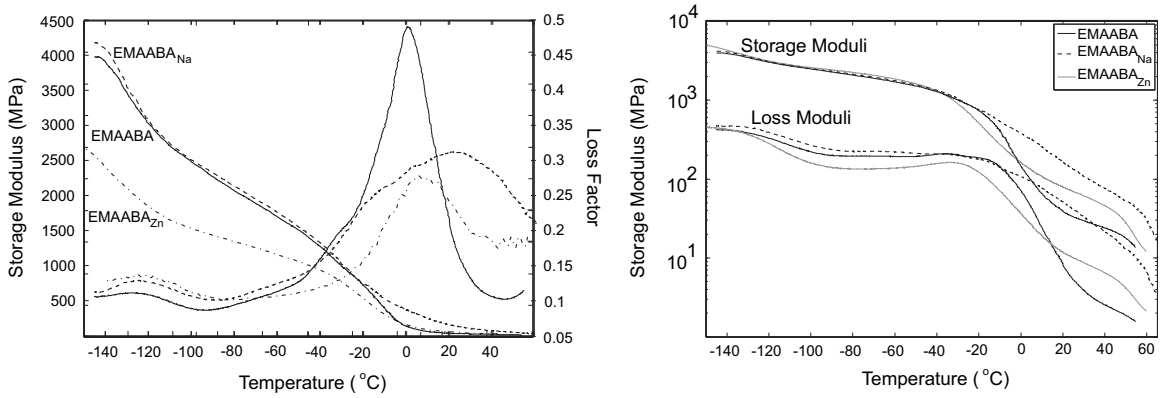

Fig. 1. Storage modulus (decreasing from left to right) and loss factor (increasing from left to right) vs. temperature for EMAABA (solid lines), EMAABA$_{Na}$ (dashed lines), and EMAABA$_{Zn}$ (dotted lines) at a frequency of 1 Hz (left). Storage and Loss moduli (logarithmic scale) vs. temperature for the three materials (right).

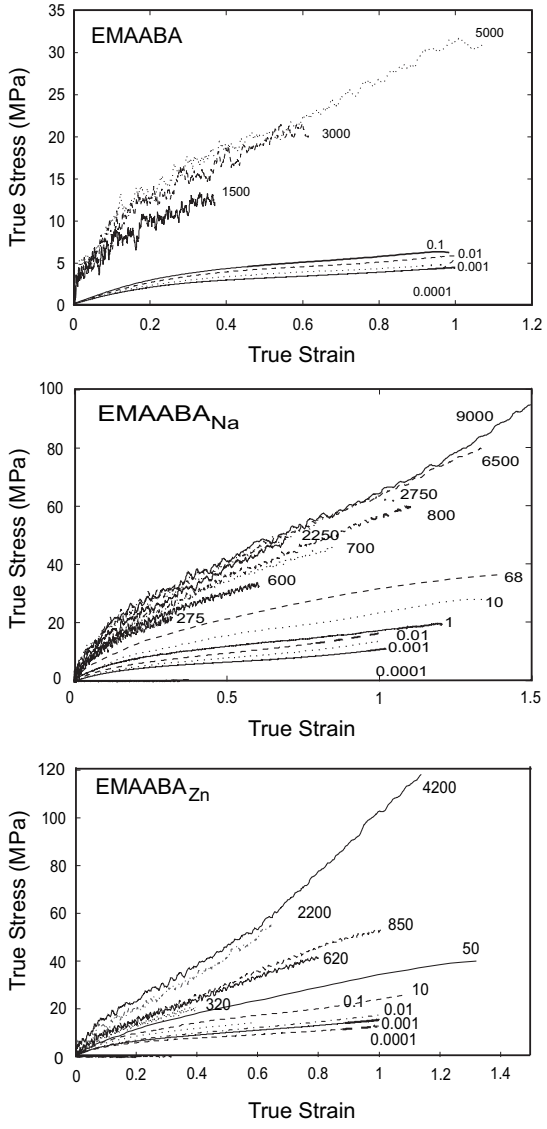

Fig. 2. Uniaxial compression true stress-true strain curves for EMAABA (top), EMAABA$_{Na}$ (center), and EMAABA$_{Zn}$ (bottom) at different strain rates.

2. Experimental protocol

2.1. Materials

The ethylene methacrylic acid butyl acrylate copolymer (EMAABA) used in this study contained 9% methacrylic acid (MAA) and 23% *n*-butyl acrylate (nBA). The EMAABA terpolymer was partially neutralized with sodium cations (53% of the acid groups neutralized with Na^+) and Zinc cations (53% of the acid groups neutralized with Zn^+) to produce ionomer forms of the polymer, herein referred to as EMAABA$_{Na}$ and EMAABA$_{Zn}$ respectively. These random copolymers with long chain branches were produced using a high pressure autoclave process. The nature of the branching in their polyethylene sections is assumed to be similar to what is found in polyethylene homopolymers [11,12] produced via similar processes. Both materials were provided by DuPont in compression molded plaques, approximately 150 mm × 150 mm × 3.15 mm. Compression specimens were punched from the plaques using special expulsion punches fabricated by the Dewes-Gumbs Die Co. For compression testing, circular punches were used, giving cylindrical samples approximately 6 mm in diameter for low-rate testing and 5 mm in diameter for high-rate testing.

2.2. Dynamic mechanical analysis

Dynamic Mechanical Analysis (DMA) was performed on a TA Instruments Q800 dynamical mechanical analyzer. Specimens were cut from the 3.15 mm thick plaque, with a width approximately

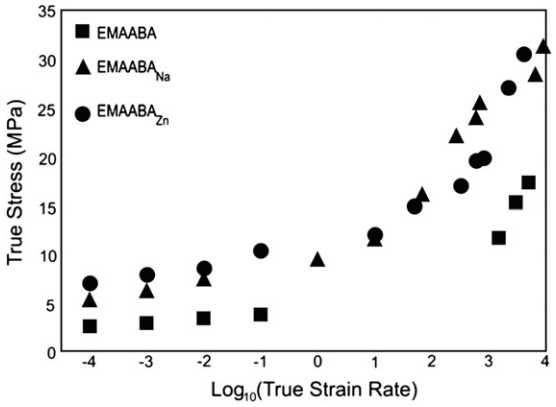

Fig. 3. True stress vs. log$_{10}$(true strain rate) for the materials at a true strain of 0.3.

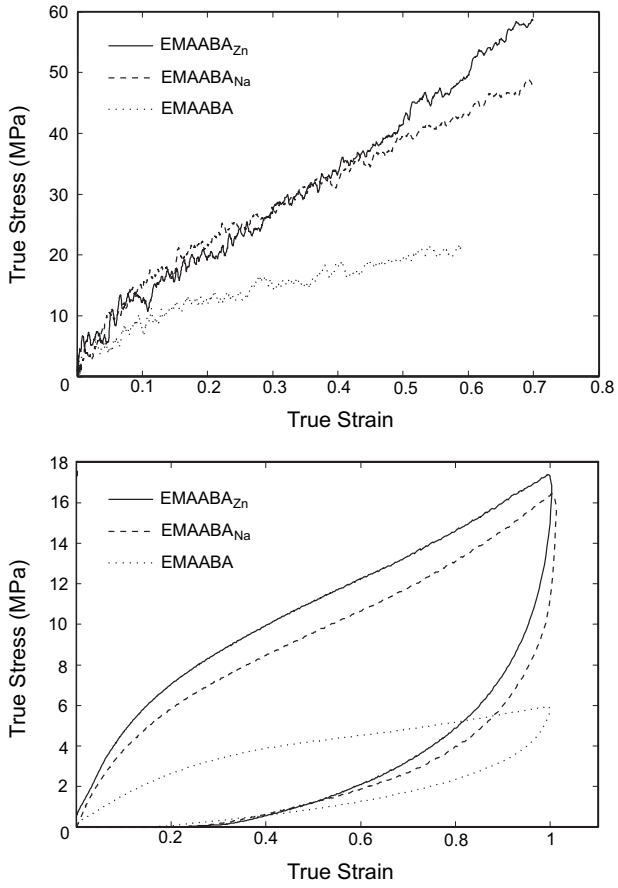

Fig. 4. True stress vs. true strain curves for the materials at a nominal strain rate of approximately 2200 s^{-1} (top) and 10^{-3} s^{-1} (bottom).

1.5 mm, and length approximately 20 mm. The specimens were tested in uniaxial tension at three different frequencies (1 Hz, 10 Hz, and 50 Hz) and a strain amplitude of $\epsilon_a = 0.2\%$ from $-150\,^{\circ}C$ to $100\,^{\circ}C$, measuring the storage modulus E', loss modulus E'', and loss factor ($\tan\,\delta = E''/E'$). The average strain rate of these tests is approximated as $\dot{\epsilon} = 2\epsilon\omega$ giving strain rates of approximately 0.004 s^{-1}, 0.04 s^{-1}, and 0.2 s^{-1}, respectively.

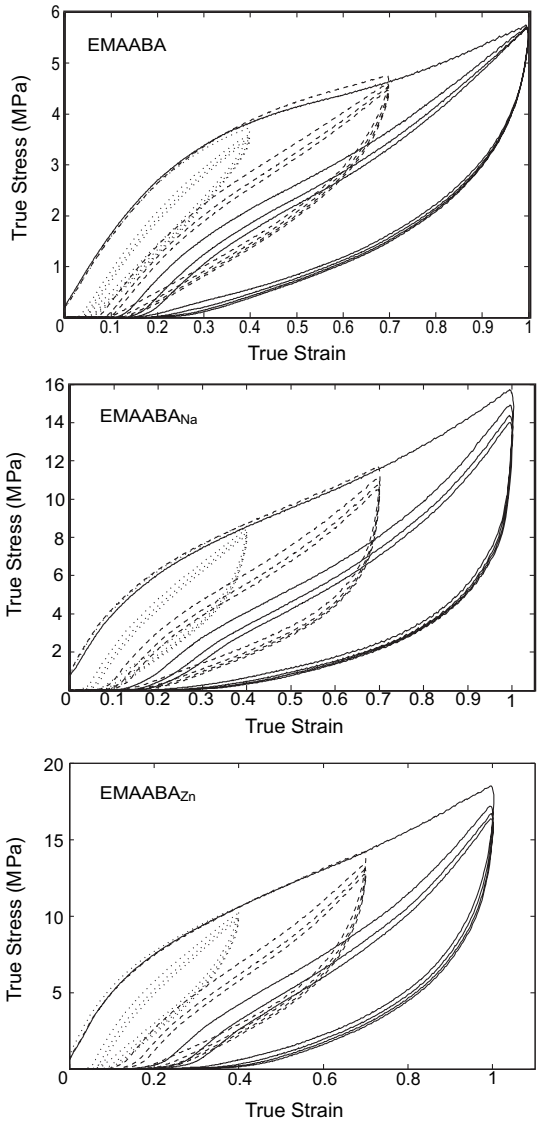

Fig. 5. Cyclic uniaxial compression tests for EMAABA (top), EMAABA$_{Na}$ (center), and EMAABA$_{Zn}$ (bottom) to/from true strains of 0.4 (dotted lines), 0.7 (dashed lines), and 1 (solid lines) and strain rate of $10^{-2}s^{-1}$.

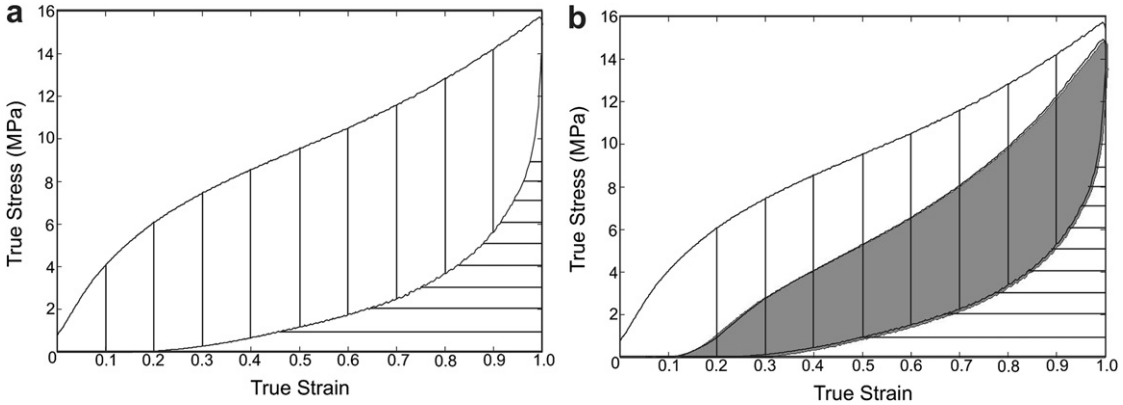

Fig. 6. Relative work density quantities for the first (a) and second (b) load cycles. The area with vertical lines corresponds to the work density dissipated in the first cycle. The area with horizontal lines correspond to the work density "recovered" after each cycle (note this quantity is approximately equivalent for both load cycles). The shaded area corresponds to the work density dissipated in the second load cycle. The total work density of each cycle is the sum of the dissipated and recovered work.

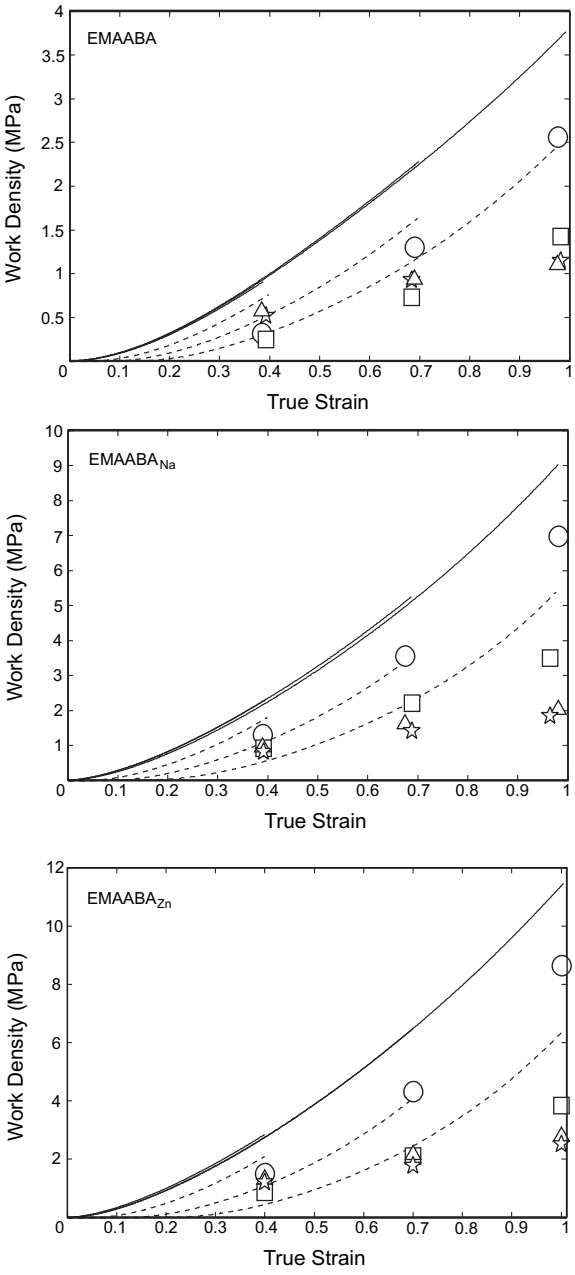

Fig. 7. Work density during the first load cycle (solid lines) and the second load cycle (dashed lines) for EMAABA (top), EMAABA$_{Na}$ (center), and EMAABA$_{Zn}$ (bottom) during cyclic loading. Specimens were loaded-unloaded-reloaded-unloaded to and from true strains of 0.4, 0.7, and 1. The dissipated work density and the recovered work density after each cycle are also plotted, where circles correspond to work dissipated in the first cycle, triangles correspond to work recovered after the first cycle, squares correspond to work dissipated in the second cycle, and stars correspond to work recovered after the second cycle.

2.3. Uniaxial compression tests

Uniaxial compression tests were performed on a Zwick mechanical testing machine (Zwick/Roell Z2.5) at nominal strain rates ranging from $10^{-4}\,s^{-1}$ to $10^{-1}\,s^{-1}$. To reduce friction, the compression platens were coated with a thin layer of petroleum jelly and thin Teflon sheets were placed between the specimen and the petroleum jelly-coated platens to ensure that the lubricant did not diffuse into the material. A camera was used during testing to monitor the specimen deformation, verifying the near homogeneity of the deformation.

For high strain rate compression tests, a split Hopkinson pressure bar (SHPB) apparatus as described in Mulliken and Boyce [13] was used. To reduce friction, both faces of the specimens were directly coated with petroleum jelly just prior to testing.

Cyclic load-unload-reload tests were performed on the Zwick mechanical testing machine. Tests were performed at an engineering strain rate of $0.01\,s^{-1}$. Separate specimens were loaded to a true strain (here defined as $\log(L/L_0)$ with L and L_0 denoting current and initial length respectively) of 0.4, 0.7, and 1, then unloaded to the initial position. Each cycle of load-unload was repeated four times, where a stable repeatable path was achieved after four cycles, with further cycles overlapping the fourth cycle.

Stress relaxation tests were also performed on the Zwick. Specimens were compressed at an engineering strain rate of $0.01\,s^{-1}$ to a true strain of 0.2, then held at that strain for 100s, during which time the stress relaxed significantly. The strain was then incrementally increased in increments of 0.2 up to a true strain of 1, held for 100s after each increment and repeated again after strain increments of 0.2 on the unloading path, the reloading path, and subsequent unloading path.

3. Experimental results

3.1. Dynamic mechanical analysis

DMA results for storage modulus (E'), loss modulus (E''), and loss factor ($\tan\delta$) at three frequencies (1, 10, and 50 Hz) over a temperature range from −150 °C to 60 °C were acquired; E', E'' and $\tan\delta$ at a frequency of 1 Hz are shown in Fig. 2 for all of the materials.

At 1 Hz, the γ-transition of EMAABA is located at a temperature of approximately −125 °C, and is associated with the local motions of linear ethylene sequences [8]. The β-transition (glass transition), is broad, extending from approximately −25 °C to 30 °C, as is evidenced by the width of the $\tan\delta$ curve. Taking the peak of the $\tan\delta$ as the glass transition temperature (T_g), the EMAABA is found to have a T_g of approximately 0 °C. Previous work has attributed the glass transition of ethylene methacrylic acid (EMAA) copolymers to a relaxation in the amorphous branched polyethylene phase [8], and here we attribute the transition to a similar mechanism in the amorphous ethylene butyl acrylate regions.

Neutralization is observed to increase storage modulus in the rubbery regime (i.e. for temperatures above ~5 °C) as well as to decrease the 'sharpness' in the drop in storage modulus in the glass transition regime giving an accompanying broadening of the loss factor. The EMAABA$_{Na}$ storage modulus in the glassy region is nearly identical to that of EMAABA, but EMAABA$_{Zn}$ exhibits a lower storage modulus in the glassy regime. At room temperature (which is in the elastomeric regime), the EMAABA$_{Na}$ and EMAABA$_{Zn}$ are stiffer than the EMAABA as is evidenced by the higher storage modulus and will be apparent in the large deformation stress-strain behavior. We postulate that the higher stiffness of the EMAABA$_{Na}$ and the EMAABA$_{Zn}$ in the "rubbery" regime is due to ionic aggregates stiffening the soft domains. Both the EMAABA$_{Na}$ and the EMAABA$_{Zn}$ show a loss modulus of similar magnitude to the EMAABA, but occurring over a broader temperature regime, suggesting that the ionic aggregates may broaden the dissipative mechanism; this broader temperature regime lends the ionomers more dissipation at 25 °C (Fig. 1). This result will also be apparent in the rate-dependent large deformation behavior.

The γ-transition of the material is relatively unaltered upon neutralization i.e. the EMAABA$_{Na}$ gives the γ-transition at −125 °C as in the neat EMAABA whereas the Zn-neutralization shows a small shift to a slightly lower temperature. The β-transition, measured using the peak of the $\tan\delta$, is slightly altered by both Na- and Zn-neutralization. For the EMAABA$_{Na}$, the β-transition shifts to

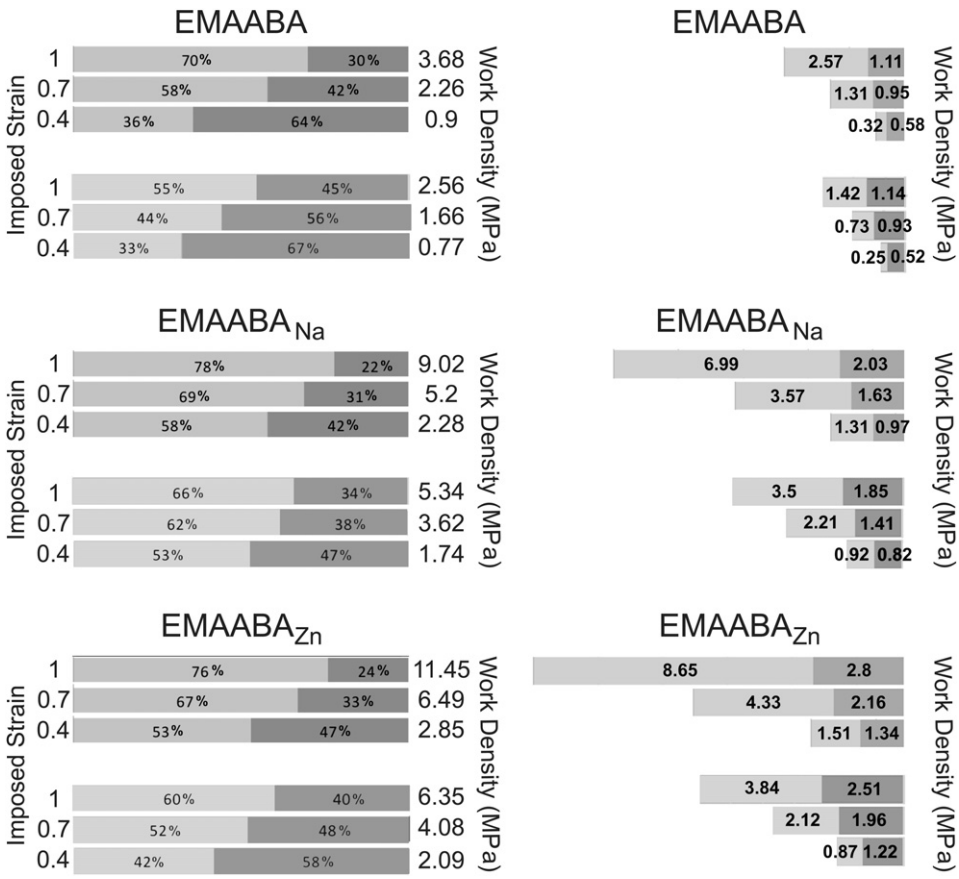

Fig. 8. (Left) Percentage of work dissipated and recovered for the three materials in two-cycle loading to different strains. The top 3 bar in each set show the first cycle, with the numbers on the left corresponding to the maximum strain, and the numbers on the right corresponding to the total work density in MPa. The bottom 3 bar correspond to the same quantities for the second load cycle. The lighter color in each bar corresponds to the work dissipated, while the darker color corresponds to the work recovered. (Right) Actual values of work density dissipated and recovered for two-cycle loading to the imposed strains shown on the left. Again, the top set of bars corresponds to the first cycle, while the bottom set corresponds to the second cycle. The lighter color corresponds to the work dissipated, while the darker color corresponds to the work recovered.

a temperature of approximately 22 °C, while for the $EMAABA_{Zn}$ the β-transition shifts to a temperature of approximately 11 °C.

3.2. Uniaxial compression tests

3.2.1. Rate-dependent monotonic large strain behavior

Fig. 2 shows the true stress-true strain behavior for EMAABA (top), $EMAABA_{Na}$ (center), and $EMAABA_{Zn}$ (bottom) when tested in uniaxial compression at 25 °C over a wide range in strain rates (from 10^{-4} s^{-1} to over 9000 s^{-1}). All three materials demonstrate a similar overall shape for their stress-strain curves, with an initially stiff region rolling over to a more compliant region. Moreover all three materials show a clear rate-dependence, with the materials exhibiting higher stress at a given strain for increasing strain rates. Fig. 3 shows the stress levels taken at a true strain of 0.3 as a function of the strain rate. At low strain rates the stress level is found to depend linearly on the logarithm of the strain rate; extrapolation of this dependency to higher strain rates reveals the data to depart from this dependency, implying the emergence of an additional deformation resistance encountered at high rates. This transition in rate dependence was discussed in Deschanel et al. [10] and is linked to the transitioning through the glass transition regime with increasing strain rate, going from the rubbery or near-rubbery regime into the leathery regime.

Fig. 4 shows a more direct comparison of the behavior of these materials at a high rate (top) and a low rate (bottom). It is clear that the strain for rollover and the nature of the rollover are similar. However, the initial and post-rollover stiffnesses of the $EMAABA_{Na}$ and $EMAABA_{Zn}$ are significantly greater than of the EMAABA. For all materials the unloading paths are highly nonlinear and show extensive recovery, exhibiting a residual strain of approximately 0.2 after an imposed strain of approximately 1. This is a clear indication that the neutralized materials are nearly as resilient as the neat material even after excursions to large strains. The loading-unloading stress-strain curves also show a clear hysteresis loop revealing that much of the work of deformation is dissipated (to be quantified further later in this paper) where the neutralized materials exhibit a dramatically greater level of dissipation compared to the neat EMAABA. Note that the unloading behavior is not obtained during testing at high rates due to the nature of the applied loading history in the SHPB.

3.2.2. Cyclic loading

The dissipative nature of the work with deformation is quantified by examining the loading, the unloading and the reloading response. Fig. 5 shows the material stress-strain behavior during cyclic compression tests to/from/to true strain levels of 0.4, 0.7, and 1 at a strain rate of $10^{-2}s^{-1}$ for the three materials. Although highly resilient, the materials do exhibit a residual strain after the first load cycle; additional recovery is observed with time after unloaded (i.e., while at zero stress) as is apparent by reloading curves beginning at a strain smaller than the strain observed immediately upon unloading. Upon reloading, a more compliant response is

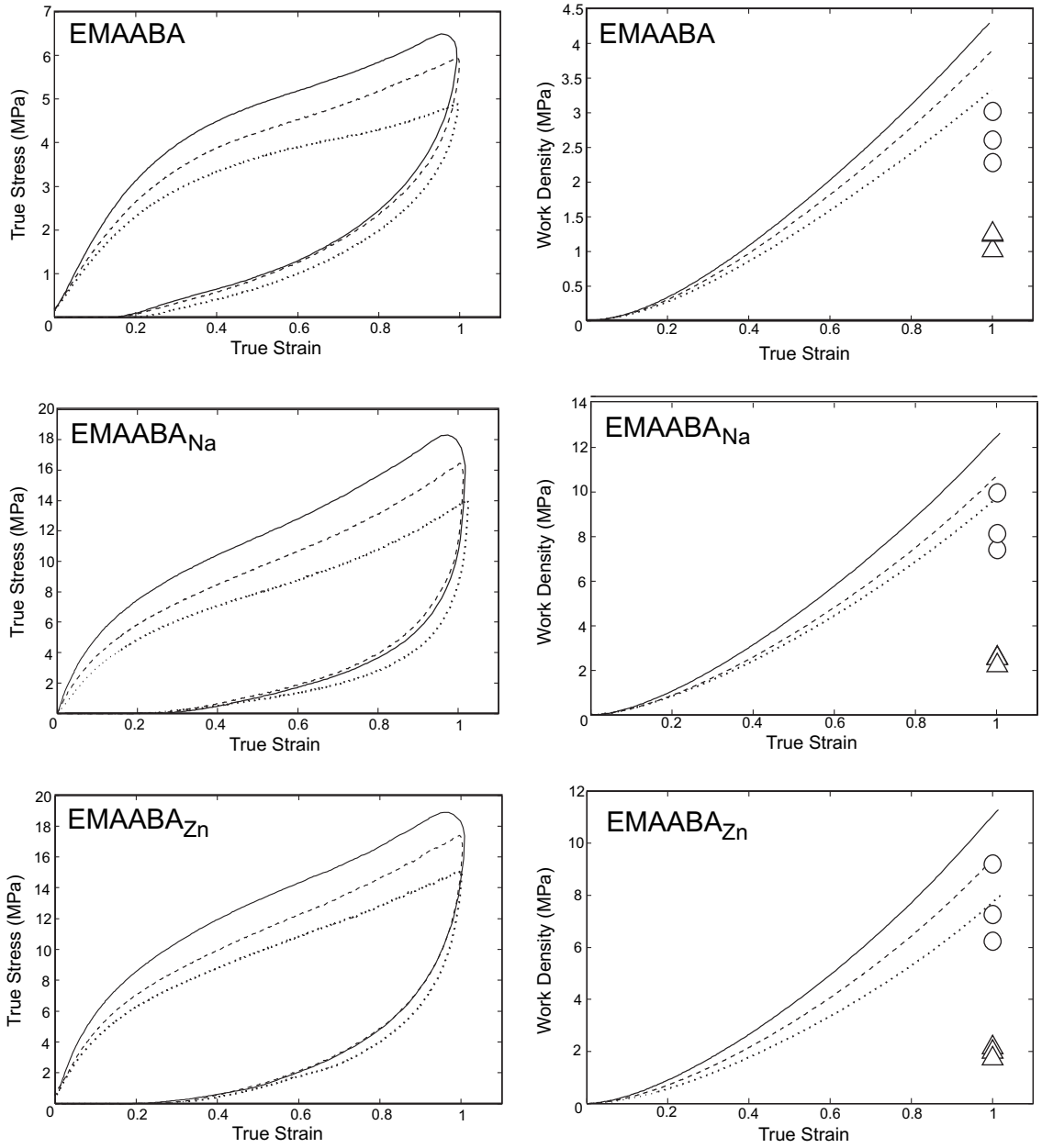

Fig. 9. (Left) true stress vs. true strain for EMAABA (top), EMAABA$_{Na}$ (middle), and EMAABA$_{Zn}$ (bottom). Solid lines correspond to tests at a nominal strain rate of 0.1 s^{-1}, dashed lines correspond to tests at a nominal strain rate of 0.01 s^{-1}, and dotted lines correspond to tests at a nominal strain rate of 0.001 s^{-1} (Right) total work, dissipated work, and recovered work for EMAABA (top), EMAABA$_{Na}$ (middle), and EMAABA$_{Zn}$ (bottom). Solid lines correspond to the total work applied to the material in cyclic loading to a true strain of 1 at a nominal strain rate of 0.1 s^{-1}. Dashed lines correspond to total work applied to the material in cyclic loading to a true strain of 1 at a nominal strain rate of 0.01 s^{-1}. Dotted lines correspond to total work applied to the material in cyclic loading to a true strain of 1 at a nominal strain rate of 0.001 s^{-1}. Circles correspond to the amount of the work that is dissipated at each strain rate; triangles correspond to the amount of work that is recovered at each strain rate.

observed where the reloading stress-strain curve rejoins the initial loading curve upon reaching the strain from which unloading began. The more compliant reloading behavior is considered a result of structural evolution/breakdown with strain producing the additional dissipation seen in the first load cycles. After unloading from the second cycle, the reloading and subsequent unloading are nearly identical to that of the first unload/reload. This indicates that the majority of the structural evolution of the material with strain occurs in the first cycle. Note that the softened behavior also leads to a dramatic reduction in the hysteresis loops for subsequent cycles when compared to the first load cycle. This strain-induced softening is found to increase significantly with imposed strain. This phenomenon is similar to that observed in vulcanized rubbers [14–17], in many copolymeric materials and other thermoplastic elastomers [18,19] and is often referred to as the Mullins effect.

The cyclic loading tests also give insights into the evolution of the yielding phenomenon in each material. As discussed above, the materials exhibit an initially stiff response, followed by a gradual rollover type of yield. In subsequent cycles, the rollover behavior is much less apparent, with the sharpness of the yield decreasing as the imposed cyclic strain increases. This yield evolution suggests a breakdown of the structural features governing initial yield.

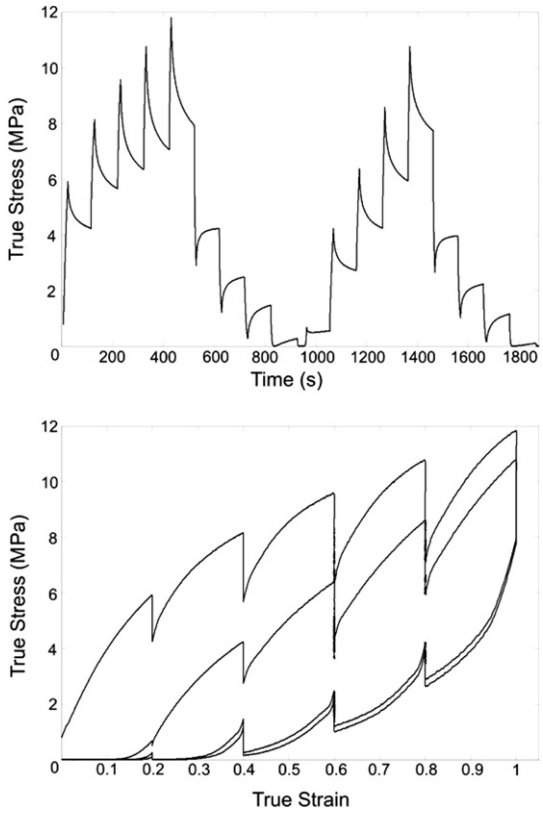

Fig. 10. Two-cycle relaxation tests for $EMAABA_{Na}$ at a nominal strain rate of 0.01 s^{-1}; true stress vs. time (top), and true stress vs. true strain (bottom) are shown.

3.2.3. Energy storage/dissipation response

As indicated earlier, cyclic testing results also provide insight into the energy dissipation features of the materials. Here, we breakdown the work density W (N-m/m^3 or MPa) of the material during loading by integrating the stress over different portions of the strain history as shown in Fig. 6. This breakdown gives the work density required to strain the material, as well as the relative amounts of work density dissipated during a load cycle and recovered after a load cycle. Here, for comparison purposes, we take the area under the unloading curve to be the 'recovered' work density, noting that dissipation occurs during loading and unloading. Fig. 6 highlights these work quantities for a test where the material is loaded-unloaded (a) and further reloaded-unloaded (b).

Fig. 7 shows the evolution of the total work, the dissipated work and the recovered work, where the dissipated and recovered quantities are plotted as discrete points at the maximum strain of its cycle. As shown in Fig. 7, focusing first on EMAABA, the dissipated work during the first cycle increases with strain in a manner similar to (but lower than) the total work evolution whereas the increase in recovered work decreases with increasing strain, indicating that the work of deformation becomes more dissipative with increasing strain. At an imposed strain of 0.4, the recovered portion (0.6 MPa) is significantly greater than the dissipated contribution (~0.3 MPa); however, this trend is reversed at large strain. For the second cycle the evolution of recovered work is essentially identical to that of the first cycle, reflecting the unloading curve being independent of cycle; however, the second cycle shows a dramatic reduction in total work, which is reflected in the dramatic reduction in dissipation for load cycles subsequent to the first cycle. The independence of recovered work with cycle and the strong dependence of magnitude of dissipated work on cycle are highlighted in Fig. 8, which discretely compares the amounts of work

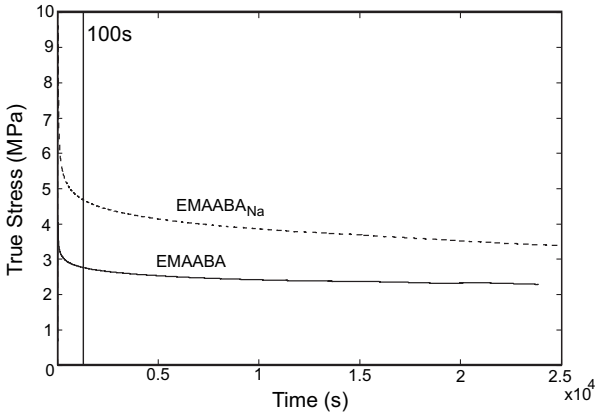

Fig. 11. True stress vs. time for long time (7 h) relaxation tests of EMAABA and $EMAABA_{Na}$. In both cases relaxation continues beyond the initial 100 s hold period (denoted with the vertical dotted line). However, in both cases, the majority of the relaxation occurs in the initial 100 s.

dissipated and recovered in both the first and second load cycle for all three materials, as well as the percentage of work dissipated and recovered. The difference in dissipation during the first and the second cycle highlights the presence of at least two dissipation mechanisms - one mechanism related to an evolution in the underlying microstructure with strain that takes place during the first cycle and the second mechanism due to local viscous and friction effects related to the observed rate-dependence of the material.

Staying focused on EMAABA, the rate effect on the total work, recovered work, and dissipation (at a strain of 1) are shown in Fig. 9 (right). The increase in work with an increase in rate is ultimately manifested as an increase in dissipation, associated with the second viscous dissipation mechanism.

The influence of the neutralization on the work quantities for $EMAABA_{Na}$ and $EMAABA_{Zn}$ are also shown in Figs. 7–9. The basic trends in evolution are similar to those of EMAABA with the exception of the dissipated portion being greater than the recovered portion even at the strain of 0.4. At the imposed strain of 0.4, the amount of dissipation due to structural evolution is modest (as evidenced by only a modest decrease in dissipation in the second cycle for $\in_{imposed} = 0.4$) and hence the dissipation up to strains of 0.4 is primarily viscous in nature, tracking with the loss modulus trends of the DMA. As the imposed strain of the first cycle is increased, the incremental increase in recovered work decreases with increase in strain (as it did in EMAABA) and hence the relative contribution of dissipation increases with an increase in strain. The second cycle contours reveal that much of the dissipation of the first cycle is due to microstructural evolution during the first loading cycle. The influence of rate on these quantities is further highlighted in Fig. 9, which shows the cyclic stress-strain curves at different rates up to a strain of 1 and the corresponding work curves; these data show that the contribution of structural evolution to dissipation is significant and that the rate-related dissipation mechanism is important.

3.2.4. Stress relaxation tests

Mechanisms of energy storage and dissipation in the stress-strain behavior are further characterized in stress relaxation tests. Specimens were compressed to true strains of 0.2, 0.4, 0.6, 0.8, and 1 with intermittent 100s hold periods (hold periods were repeated in the unloading and reloading cycles as well), monitoring the stress as function of strain and time. Fig. 10 shows the true stress vs. time history (top) as well as the true stress vs. true strain plot

(bottom) for $EMAABA_{Na}$, where the results shown for this material are also indicative of the behaviors of EMAABA and $EMAABA_{Zn}$.

The stress changes significantly during the strain hold periods: during loading holds, the stress decreases with time and during unloading holds, the stress increases with time. The rate of change decreases with time, approaching a plateau value that depends on the magnitude of applied strain.

Comparing the relaxation at different strains during loading, unloading and reloading, we observe the following key behaviors: (1) during unloading holds, the stress rises to a noticeably lower stress level than it had relaxed at the same strain hold during the initial loading - a consequence of the softening of the equilibrium elastic behavior of these materials that occurred during loading; (2) during reloading holds, the stress relaxes to a significantly lower level of stress at any given strain than observed during the first-cycle loading – again a result of the softening due to structural breakdown during the initial loading cycle; (3) during reloading holds, the stress relaxes to a similar plateau stress level as approached during relaxation during unloading – a result of the microstructure of the material during unloading and that present during reloading being in essentially the same "softened" state; and (4) the relaxation periods during the second unloading track the behavior observed during the unloading of the first cycle, again showing that the structure evolution occurs during the initial loading cycle.

Finally, it is clear from Fig. 10 that the material does not achieve a plateau stress value during the 100s hold period. Thus, tests were conducted using long holding time periods (approximately 7 h) to determine if the material did indeed come to equilibrium plateau value. The corresponding stress-time curves are shown in Fig. 11 and demonstrate that there is a very small (but non-zero) amount of relaxation occurring beyond the initial 100s period.

4. Discussion and conclusions

The ethylene methacrylic acid butyl acrylate terpolymers are characterized by an excellent combination of mechanical properties that can be tailored by neutralization, including a relatively stiff initial response, a reasonably high level strength (load bearing level) for an elastomer and extensive dissipation, all while retaining significant resiliency even after large strain excursions.

EMAABA demonstrates a strongly rate-dependent initial stiffness, ranging from approximately 10–75 MPa for strain rates ranging from 10^{-4} to 5000 s^{-1}. At a strain of approximately 0.2, the material demonstrates a smooth rollover to a more compliant large deformation behavior. Unloading reveals a significant hysteresis loop and a moderate residual strain ($\sim$0.2 after a strain of 1.0), demonstrating the dissipative yet resilient behavior of these materials. For additional load cycles, the material is more compliant, with less work dissipated in the second cycle as compared to the first cycle, yet with nearly identical recovery behavior. Similar behaviors are observed in the neutralized materials $EMAABA_{Na}$ and $EMAABA_{Zn}$, where neutralization increases the stiffness, the strength, and the dissipation yet retains the resiliency.

Relaxation tests show significant time dependence for all materials. Moreover at a given strain, the change in stress with time is found to be strongly dependent on cycle (i.e., whether the strain hold occurs during loading, unloading or reloading). In addition to showing the time dependence of stress due to viscoelasticity, the results also reinforce conclusions drawn from the earlier cyclic loading results, namely that a new softened structure is established during the initial load excursion.

The rate-dependent stress-strain curves, the cyclic loading curves, and the relaxation results highlight the existence of two major dissipation mechanisms in these materials. The first is a conventional viscoelastic mechanism which is evidenced by the material rate-dependence, the relaxation response, and the presence of dissipation in later cycles of multiple-cycle loading. The second is a result of the microstructural evolution/breakdown incurred during large-deformation loading. This mechanism is evidenced by the more compliant response of the material in the second load cycle (relative to the first), the dramatic reduction in the hysteresis loop after the first cycle of loading and the relaxation behavior during unloading and reloading where at a given strain the stress relaxes to a lower level than observed during the initial load cycle. The structural breakdown mechanism provides a powerful dissipation mechanism beyond viscoelasticity for applications - such as adhesion, abrasion resistance, puncture resistance and impact loading - which require dissipation while still exhibiting a relatively stiff small strain behavior and still retaining resiliency after large strain excursions.

The influence of neutralization on these features shows that varying ionic content enables the tailoring of these properties for the particular application. Therefore neutralization give us the opportunity to mimic nature, where protein-rich materials such as spider silk [20–22] and mussel byssal threads [23–26] have been shown to exhibit the same combinations of mechanical properties - initially stiff behavior, strong hysteresis, cyclic softening (structural breakdown) and yet extensive recovery after large strain - which they tailor by varying the material's protein fiber content.

Acknowledgements

The authors acknowledge the generous support of the DuPont-MIT Alliance.

References

[1] Eisenberg A, Kim J. Introduction to ionomers. New York: John Wiley & Sons, Inc; 1998.
[2] Akimoto HA, Kanazawa T, Yamada M, Matsuda S, Shnaike GO, Murakami AJ. Appl Polym Sci 2001;81:1712–20.
[3] Longworth R, Nagel H. Packaging. In: Tant MR, Mauritz KA, Wilkes GL, editors. Ionomers: synthesis, structure, properties, and applications. London: Blackie Academic and Professional; 1997. p. 365.
[4] MacKnight WJ, Earnest TR. J Polym Sci Macromolecular Rev 1981;16:41–122.
[5] Tant MR, Wilkes GL. J Material Sci Macromolecular Chem Phys 1988;C28:1–63.
[6] Kinsey RH. Appl Polym Symposia 1968;11:77–94.
[7] Scogna RC, Register RA. Polymer 2009;50:585–90.
[8] MacKnight WJ, McKenna LW, Read BE. J Appl Phys 1967;38(11):4208–12.
[9] Scogna RC, Register RA. Polymer 2008;49:992–8.
[10] Deschanel S, Greviskes BP, Bertoldi K, Sarva SS, Chen W, Samuels SL, et al. Polymer 2009;50(1):227–35.
[11] Ehrlich P, Mortimer G. Fortschritte der Hochpolymeren-Forschung; 1970:386–448.
[12] Woodbrey JC, Ehrlich P. J Am Chem Soc 1963;85(11). 1580-&.
[13] Mulliken AD, Boyce MC. Int J Solids Structures 2006;43(5):1331–56.
[14] Mullins L, Tobin NR. J Appl Polym Sci 1965;9:2993–3010.
[15] Harwood JAC, Mullins L, Payne AR. J Appl Polym Sci 1965;9:3011–21.
[16] Harwood JAC, Payne AR. J Appl Polym Sci 1966a;10:315–24.
[17] Harwood JAC, Payne AR. J Appl Polym Sci 1966b;10:1203–11.
[18] Yi J, Boyce MC, Lee GF, Balizer E. Polymer 2006;47:319–29.
[19] Qi HJ, Boyce MC. Mechanics Mater 2005;37:817–39.
[20] Gosline JM, Guerette PA, Ortlepp CS, Savage KN. J Exp Biol 1999;202:3295–303.
[21] Denny M. J Exp Biol 1976;65:483–506.
[22] Carrington E. Trends Biotechnol 2008;26:55–7.
[23] Bell E, Gosline JM. J Exp Biol 1996;199:1005–17.
[24] Coyne KJ, Qin XX, Waite JH. Science 1997;277:1830–2.
[25] Bertoldi K, Boyce MC. J Mater Sci 2007;42:8943–56.
[26] Greviskes B. Thesis (S.M.)-Massachusetts Institute of Technology: Dept. of Mechanical Engineering; 2009.